Journal of Solid State Chemistry 182 (2009) 1754–1760

Contents lists available at ScienceDirect

Journal of Solid State Chemistry

journal homepage: www.elsevier.com/locate/jssc

The clathrate $Ba_8Cu_xGe_{46-x-y}\square_y$: Phase equilibria and crystal structure

Nataliya Melnychenko-Koblyuk [a], Andriy Grytsiv [a], Peter Rogl [a,*], Harald Schmid [a], Gerald Giester [b]

[a] Institute of Physical Chemistry, University of Vienna, A-1090 Wien, Austria
[b] Institute of Mineralogy and Crystallography, University of Vienna, A-1090 Wien, Austria

ARTICLE INFO

Article history:
Received 4 February 2009
Received in revised form
3 April 2009
Accepted 4 April 2009
Available online 23 April 2009

Keywords:
Clathrate type I structure
$Ba_8Cu_xGe_{46-x-y}\square_y$
Phase equilibria
XPD
XSCD

ABSTRACT

Phase relations at 700 °C, 800 °C and solidus temperatures have been derived for the clathrate system $Ba_8Cu_xGe_{46-x-y}\square_y$ via X-ray single crystal and powder diffractometry combined with electron probe micro analysis and differential thermal analysis. The ternary clathrate phase derives from binary $Ba_8Ge_{43}\square_3$ and extends up to $x = 6$. Structure investigations define cubic primitive symmetry with the space group type $Pm\bar{3}n$ consistent with a clathrate type I structure throughout the entire homogeneity region $0 < x \leqslant 6$ but defect-free $Ba_8Cu_xGe_{46-x}$ exists for $x \geqslant 5.5$.

1. Introduction

Early interest in clathrate type I compounds stems from superconducting properties, discovered in Ba_8Si_{46} (8 K, [1]) and pertinent to M = Cu, Ag, Au-substituted clathrates $Ba_8M_xSi_{46-x}$ for small amounts of x. Electronic structure calculations gave hints that superconductivity in Ba and Ge based clathrate I may only appear in defect-free Ge-framework structures [2]. First principles calculations also showed that clathrates $Ba_8\{Cu,Ag,Au\}_6Si_{40}$ are degenerate semiconductors with p-type carriers and with Seebeck-coefficients of ~100 μV/K below 1000 K [3,4]. Extensive information on crystal structure and thermoelectric properties of the clathrates are available from recent reviews [5].

In our recent work on Ba-, Si-, and Ge-based clathrate systems $Ba_8M_x\{Si,Ge\}_{46-x-y}\square_y$ (M = Pd, Pt, Zn, Cd; □ = vacancy), we have shown that (a) M-atoms substitute for framework atoms reducing the concentration of vacancies in the crystal structure and (b) increasing M-content drives the metallic system towards a metal-to-insulator transition yielding interesting thermoelectric behaviour [6–10]. The present paper extends our systematic investigation towards the system Ba–Cu–Ge, for which a type I clathrate $Ba_8Cu_6Ge_{40}$ has first been described by Cordier [11]. Although the clathrate has been confirmed [2,12–16] and Cu/Ge exchange has been described [2,13–15] some discrepancies exist (i) concerning the extent of the homogeneity region ($x \leqslant 6$ for alloys quenched from the melt [11]; $x \leqslant 6$, quenched from 700 °C [14,15]; but $4.9 \leqslant x \leqslant 5.3$ quenched from 700 °C [2,13]) and (ii) concerning the lattice parameters of Li et al. [2,13], which severely deviate from those reported for the binary $Ba_8Ge_{43}\square_3$ by [17,18] but also for the ternary reported by [11,14–16]. X-ray powder diffraction data for alloys $Ba_8Cu_xGe_{46-x}$ (x = 2, 4, 6) were claimed to reveal about 9% defects in the 6*d* sites (Cu,Ge-atoms) for $x = 2$ and 4, respectively, as well as about 7% defects for Ba-atoms in the 6*c*-sites for $x = 6$ [2]. Although lattice parameters showed an almost linear decrease from $x = 2$ to 6, X-ray data refinement and EPMA indicated a reduced homogeneity region $4.9 \leqslant x \leqslant 5.4$ [13]. Consequently the $x = 6$ alloy was said to contain "Ge_3Cu_5" as a secondary phase [13], which, however, is hitherto unknown in the Cu–Ge binary system [19]. The findings are in contrast to a single crystal study [11] of $Ba_8Cu_6Ge_{40}$ as well as detailed X-ray powder studies [14,15] on $Ba_8Cu_xGe_{46-x}$ ($5.3 \leqslant x \leqslant 6$), a synchrotron powder investigation ($x = 5.9$ [15]) and a powder study for $x = 6$ [16], which all concluded the absence of defects in both the Ba (6c) as well as in the 6d site.

Literature information on the Ba–Cu–Ge system concerns only the formation of two ternary compounds $Ba(Cu_xGe_{1-x})_2$ ($0.33 < x < 0.5$, AlB_2-type, [20]) and $BaCu_9Ge_4$ ($LaFe_9Si_4$-type, [21]). Furthermore, there is little information on ternary phase relations concerning the two clathrates, types I and IX. Therefore the present research work attempts to (i) elucidate formation and homogeneity region of the clathrates, (ii) their phase relations at 700 and 800 °C to the surrounding phases as well as (iii) a precise description of the crystal chemistry of the entire clathrate type I solid solution $Ba_8Cu_xGe_{46-x-y}\square_y$.

2. Experimental

About 20 alloys with a weight of 1–2 g were prepared by arc-melting (weight loss less than 0.1 wt%) on a water-cooled copper

* Corresponding author. Fax: +43 1 4277 95245.
E-mail address: peter.franz.rogl@univie.ac.at (P. Rogl).

0022-4596/$ - see front matter © 2009 Elsevier Inc. All rights reserved.
doi:10.1016/j.jssc.2009.04.006

hearth in Ti-gettered argon from elemental ingots with minimal purity of 99.9 wt% (for sample location see Fig. 1). The alloys were sealed in evacuated quartz tubes and annealed at 700 and 800 °C for 7 days before quenching in cold water. Isothermal reaction temperatures were derived from thermal arrests determined in a calibrated Netzsch STA 409 PG/4/G Luxx differential scanning calorimeter (DSC) employing a heating rate of 5 K/min in Al_2O_3 crucibles under a stream of 6N argon. Prior to DTA the alloys were annealed at 600 °C for 10 days. Details on the various techniques such as electron probe microanalysis (EPMA, binary compounds (Ba_8Ge_{43} and Ba_6Ge_{25} and ternary τ_2-$BaCu_9Ge_4$ were used as standards), of X-ray diffraction techniques (X-ray powder (XRPD) and single crystal (XRSD) diffraction have been described in detail by [6,7]. Reproducibility of the EPMA measurements (at least 5 measurement for every phase) was better than 0.2 at%. Compounds Ba_8Ge_{43}, Ba_5Ge_{26} and $BaCu_9Ge_4$ were used as EPMA standards.

3. Results and discussion

3.1. Phase equilibria in the Ge–Cu_3Ge–$BaGe_2$ region of the Ba–Cu–Ge system

Whilst the binary diagram Cu–Ge is accepted after [19,22], phase equilibria for Ba–Ge were taken from [23]. To elucidate the phase relations in the Ge-rich part of the Ge–Cu_3Ge–$BaGe_2$ subsystem at $T = 800$ °C, we investigated the ternary clathrate type I solution extending from binary $Ba_8Ge_{43}\square_3$. Thus alloys with nominal composition $Ba_8Cu_xGe_{46-x}$ ($x = 0$, 2, 4, 5, and 6; see sample location in Fig. 1) annealed at $T = 800$ °C were examined by means of XRPD and EPMA. The maximal solubility of 10.9 at% Cu at $T = 800$ °C in $Ba_8Cu_xGe_{46-x-y}\square_y$ corresponds to six Cu atoms per unit cell and was established by EPMA from multiphase ternary samples with higher Cu-content. The value for the Cu-limit in the clathrate phase, $a = 1.06868(2)$, is close to that

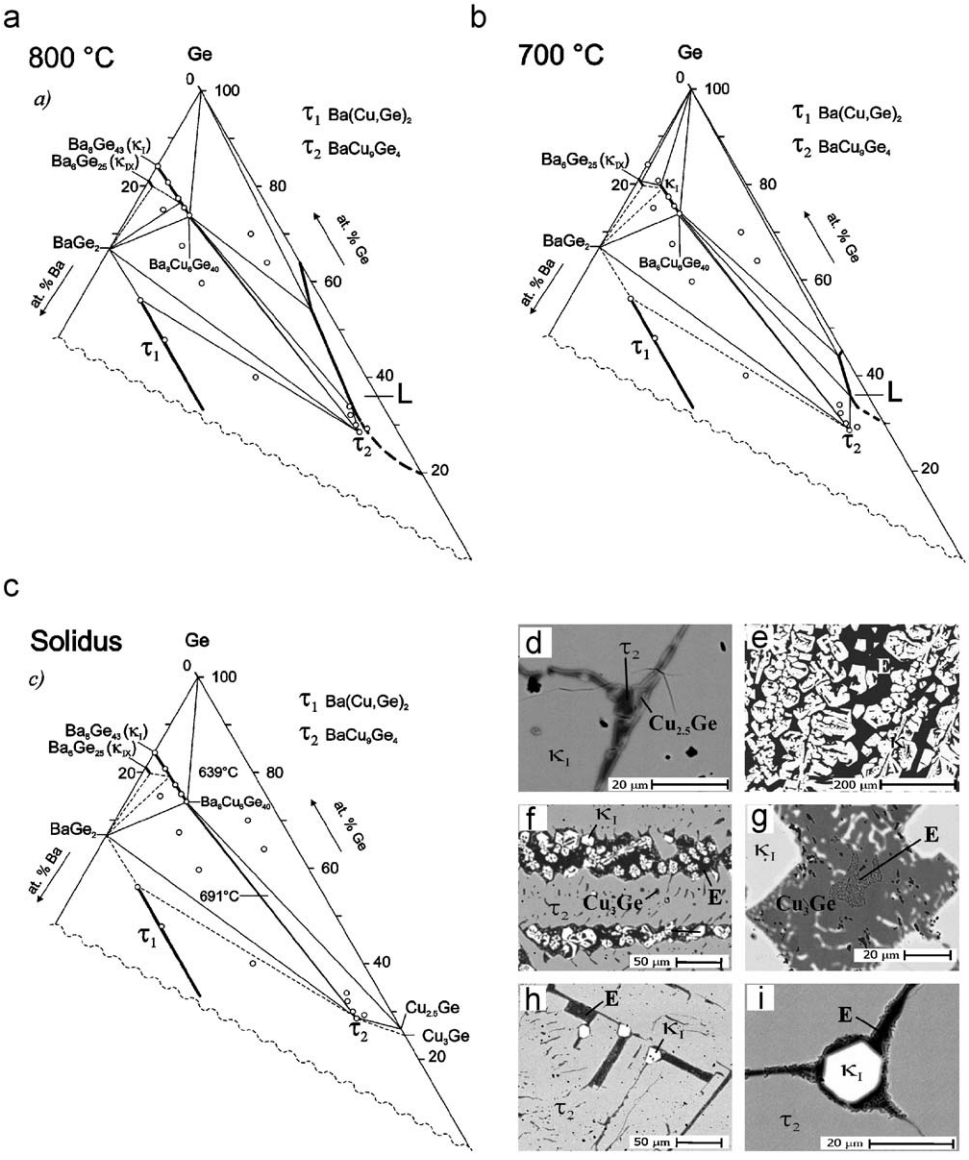

Fig. 1. Partial isothermal sections at 700 °C (a), 800 °C (b) and solidus (c) of Ba–Cu–Ge ternary system in the region Cu_3Ge–Ge–$BaGe_2$. Microstructures of $Ba_{14.8}Cu_{11.1}Ge_{74.1}$ (d, as cast), $Ba_6Cu_{30}Ge_{64}$ (e, as cast), $Ba_6Cu_{60}Ge_{34}$ (f, as cast; g, 700 °C), $Ba_7Cu_{63}Ge_{30}$ (h, as cast; i, 800 °C).

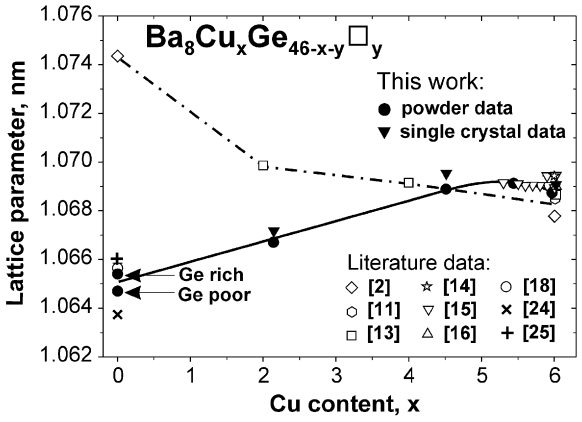

Fig. 2. Lattice parameters vs. Cu-content for $Ba_8Cu_xGe_{46-x-y}\square_y$ [24,25].

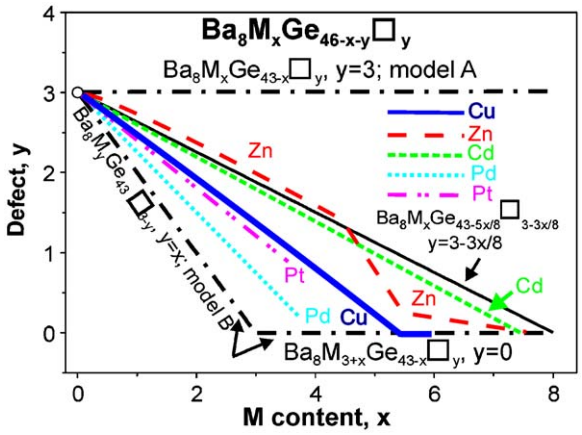

Fig. 3. Dependences of deficiency on *M*-content (M = Cu, Pd, Pt, Zn, and Cd) in $Ba_8M_xGe_{46-x-y}\square_y$ are compared for two boundary models of incorporation of *M* atoms in the lattice of $Ba_8Ge_{43}\square_3$.

reported by Cordier et al. [11] ($a = 1.06859(8)$ nm) as well as to the values by [15] ($a = 1.06894(2)$ nm), [13] ($a = 1.06872(1)$ nm), and [16] ($a = 1.06850(1)$ nm) for the clathrate composition given as "$Ba_8Cu_6Ge_{40}$" (see Fig. 2). EPMA data on alloys that were quenched from 800 °C showed a continuous solid solution deriving from binary $Ba_8Ge_{43}\square_3$ and ending in the ternary at a maximal content of six Cu atoms per formula unit. As the binary clathrate Ba_8Ge_{43} only exists in a small temperature region from 770 to 810 °C [18], the stability range of ternary $Ba_8Cu_xGe_{46-x}$ was investigated at lower temperatures. Indeed, annealing the sample with nominal composition $Ba_8Cu_4Ge_{42}$ at 700 °C for 10 days or even at 500 °C for 150 days in both cases confirmed the clathrate type I. The maximal solubility of Cu in $Ba_8Cu_xGe_{46-x}$ at $T = 700$ °C was found to be $x = 6$ (10.88 at% from EPMA). Thus we may conceive Cu-insertion and/or Cu/Ge substitution as a significant increase of thermodynamic stability for the clathrate solution. The sample with low Cu-content, $Ba_8Cu_2Ge_{44}$, consists of two phases (κ_I+Ge) in as-cast state and after anneal at 800 °C but heat treatment at 700 °C results in formation of κ_{IX} with composition $Ba_6Cu_xGe_{25-x}$, $x = 0.37$ (1.2 at% Cu). Clathrate I in this equilibrium, κ_I+κ_{IX}+(Ge), contains 4.5 at% Cu yielding the formula $Ba_8Cu_xGe_{46-x}$ with $x = 2.4$ being significantly lower than the value of $x = 4.9$ reported by [2,13] for a minimal solubility of Cu in κ_I at 700 °C. Furthermore the unit cell lattice parameter for κ_I in this sample ($a = 1.06702$ nm) perfectly fits to the compositional dependence of the lattice parameters of the clathrate obtained from samples annealed at 800 °C (Fig. 2).

The decrease of the Ba content with increasing Cu-content in the clathrate I solution, as measured by EPMA, is associated with the change in the vacancy concentration in the crystal lattice. X-ray refinements proved a complete Ba-sublattice (2*a* and 6*d* sites), therefore the vacancy concentration in the framework of the structure can be calculated from EPMA data. The amount of vacancies decreases almost linearly with increasing Cu content up to about 5.5 Cu-atoms per formula unit leaving no vacancies in the lattice for the rest of the solid solution up to $Ba_8Cu_6Ge_{40}$ (Fig. 3).

Evaluation of the phase relations at 800 °C (see Fig. 1 and Table 1) revealed the existence of two ternary compounds, τ_1-$Ba(Cu_xGe_{1-x})_2$ with the AlB_2-type structure in an extended homogeneity region at constant Ba-content and τ_2-$BaCu_9Ge_4$ at stoichiometric composition ($a = 0.83378(1)$ nm, $c = 1.20185(3)$ nm; space group $I4/mcm$) with the ordered $LaFe_9Si_4$ structure.

To evaluate the equilibria between clathrate type I (κ_I) and type IX (κ_{IX}, Ba_6Ge_{25}) we have prepared the alloys $Ba_6Cu_2Ge_{23}$ and $Ba_6Cu_4Ge_{21}$. However, samples in as-cast and annealed state (800 °C) decompose quickly due to the presence of moisture sensitive $BaGe_2$. Therefore, specimens were washed in diluted H_2SO_4 from decomposition products (brown powder), and XRPD showed that the residual powder consists entirely of clathrates type I. As no clathrate type IX was detected by XRPD, the solubility of Cu in type IX clathrate is estimated to be below 1 atom per unit cell.

Phase equilibria are presented as partial isothermal sections at 700, 800 °C and solidus in Fig. 1 (Table 1) and show tie-lines between clathrate type I (κ_I) and τ_2-$BaCu_9Ge_4$ indicating higher stability for this join with respect to $BaGe_2$+CuGe-rich liquid, which at 800 °C covers a significant part of the isothermal section. Clathrate κ_I exhibits an extended homogeneity region and crystallizes directly from liquid. Microstructure of as-cast alloy $Ba_{14.8}Cu_{11.1}Ge_{74.1}$ (Fig. 1d) reveals almost single phase clathrate with 10.3 at% Cu, a small quantity of τ_2 and traces of a phase that was difficult to identify by EPMA and XRPD. Most likely it is Cu_3Ge that was detected in equilibrium with κ_I and τ_2 after heat treatment of the sample at 800 °C. The liquids of κ_I extends at least to 30 at% Cu and one can see primary crystallization of the clathrate in $Ba_6Cu_{30}Ge_{64}$ (Fig. 1e). At higher Cu-content we observe primary crystallization of τ_2. Thus the microstructure of as-cast $Ba_6Cu_{60}Ge_{34}$ (Fig. 1f) shows big primary grains of τ_2 with tiny precipitates of Cu_3Ge or $Cu_{2.5}Ge$; the final portion of the liquid crystallizes with formation of κ_1 and a eutectic structure. Annealing of the specimen at 700 °C significantly changes the morphology of the sample (Fig. 1g). At this temperature the sample was in liquid–solid state: big grains of κ_1 and τ_2 were grown in equilibrium with a (Cu,Ge)-rich liquid that crystallises on cooling with formation of Cu_3Ge ($Cu_{75.8}Ge_{24.2}$ after EPMA) and a eutectic with composition $Ba_{0.4}Cu_{67.3}Ge_{32.3}$. This composition agrees well with the binary eutectic reaction: $l \rightarrow Cu_{2.5}Ge$+(Ge) at ~64 at% Cu [19,22].

DTA of single-phase $BaCu_4Ge_9$ indicates a single thermal arrest at 866±3 °C corresponding to the congruent melting of τ_2. Congruent formation of τ_2 is also documented in Figs. 1h and i (sample $Ba_7Cu_{63}Ge_{30}$). Similarly to $Ba_6Cu_{60}Ge_{34}$ we observe in this as-cast sample precipitation of Cu_3Ge ($Cu_{2.5}Ge$) inside the primary grains of τ_2. The precipitates disappear after annealing at 700 or 800 °C.

From the data available we were able to derive the solidus surface and to attribute the thermal arrests observed by DTA (Fig. 1c). The ternary eutectic, L→κ_1+$Cu_{2.5}Ge$+(Ge), is detected at 639±3 °C, very close to the value of 644 °C reported for the binary

Table 1
Three phase equilibria, lattice parameters, and phase composition of Ba–Cu–Ge system.

Phase region temperature	Phase	Structure type	Lattice parameters (nm)			EPMA (at.%)		
			a	*b*	*c*	Ba	Cu	Ge
800 C								
κ_I+(Ge)+L	κ_I	K_4Ge_{23-x}	1.06889(2)	–	–	14.5	10.9	74.6
	(Ge)	C_{diam}	0.56561(4)	–	–	–	–	100
	L	–	–	–	–	3.0	43.0	54
κ_I+κ_{IX}+$BaGe_2$	κ_I	K_4Ge_{23-x}	1.06893(6)	–	–	14.8	8.3	76.9[a]
	κ_{IX}	Ba_6Ge_{25}	1.4556(1)	–	–	19.4	0.5	80.1[b]
	$BaGe_2$	$BaSi_2$	0.9047(3)	0.6818(3)	1.16356(2)	–	33.3	66.7[b]
κ_I+τ_2+L	κ_I	K_4Ge_{23-x}	1.06889(2)	–	–	14.5	10.9	74.6
	τ_2	$LaFe_9Si_4$	0.83415(6)	–	1.2033(2)	7.1	64.3	28.6
	L					5.8	60.9	33.3
κ_I+τ_2+$BaGe_2$	κ_I	K_4Ge_{23-x}	1.06893(6)	–	–	14.5	10.9	74.6
	τ_2	$LaFe_9Si_4$	0.83438(7)	–	1.2043(9)	7.1	64.3	28.6
	$BaGe_2$	$BaSi_2$	0.9047(3)	0.6818(3)	1.16356(2)	–	33.3	66.7[b]
τ_1+τ_2+$BaGe_2$	τ_1	AlB_2	0.42977(4)	–	0.4979(1)	10.6	32.9	56.5
	τ_2	$LaFe_9Si_4$	0.83444(7)	–	1.2044(3)	7.1	64.3	28.6
	$BaGe_2$	$BaSi_2$	0.9096(12)	0.68122(1)	1.1643(9)	–	33.3	66.7[b]
700 °C								
κ_I+(Ge)+L	κ_I	K_4Ge_{23-x}	1.06880(2)	–	–	14.5	10.9	74.6
	(Ge)	C_{diam}	0.56561(4)	–	–	–	–	100
	L	–	–			1.7	54.8	43.5
κ_I+κ_{IX}+(Ge)	κ_I	K_4Ge_{23-x}	1.06702(1)	–	–	14.9	4.5	80.6
	κ_{IX}	Ba_6Ge_{25}	1.4538(1)	–	–	19.1	1.2	79.7
	(Ge)	C_{diam}	0.56573(2)		–	100	–	–
κ_I+τ_2+*L*	κ_I	K_4Ge_{23-x}	1.06882(2)	–	–	14.5	10.9	74.6
	τ_2	$LaFe_9Si_4$	0.83415(6)	–	1.2033(2)	7.1	64.3	28.6
	L	–	–			3.4	60.9	35.7
κ_I+τ_2+$BaGe_2$								
	κ_I	K_4Ge_{23-x}	1.06879(2)	–	–	14.5	10.9	74.6[a]
	τ_2	$LaFe_9Si_4$	0.83428(7)	–	1.2043(9)	7.1	64.3	28.6[b]
	$BaGe_2$	$BaSi_2$	0.9047(3)	0.6818(3)	1.16356(2)	–	33.3	66.7[b]

[a] Composition was estimated from lattice parameters of the clathrate phase (Fig. 2).
[b] Estimated composition. No EPMA data available due to decomposition of $BaGe_2$

reaction $l \rightarrow Cu_{2.5}Ge$+(Ge). The ternary invariant reaction, associated with the binary eutectoid, $Cu_{2.5}Ge \rightarrow Cu_3Ge$+(Ge) at 614 °C, is recorded at 618 ± 3 °C.

3.2. Crystal chemistry of the clathrate type I solid solution $Ba_8Cu_xGe_{46-x}\square_y$

For a concise picture on the structural chemistry of the clathrate type I solid solution $Ba_8Cu_xGe_{46-x}\square_y$ we attempted to evaluate atom site preferences from room temperature X-ray powder diffraction data for samples with $x = 0$, 2, 4, 5, and 6 assisted by X-ray intensity data from single crystals, which were selected from mechanically crushed samples with composition $x = 2.1$, 4.5, and 6.0 (after EPMA). In all cases extinctions were consistent with a primitive cubic lattice (space group $Pm\bar{3}n$, $a \sim 1.1$ nm) and indicated isotypism with the structure of clathrate type I. No extra reflections suggesting a larger unit cell $a' = 2a$ as reported by [18] were detected in the investigated crystals. The strongly scattering barium atoms were unambiguously located in sites 2*a* (0,0,0) and 6*c* ($\frac{1}{4}$, 0, $\frac{1}{2}$). Whereas the electron density distribution for both lattice sites 16*i* and 24*k* revealed constant electron densities, the number of electrons in the 6*d* site increased with increasing Cu content. In binary $Ba_8Ge_{43}\square_3$ [18] vacancies are located at the 6*d* site in an ordered arrangement thus giving rise to the eightfold supercell ($a' = 2a$). As refinement of occupancies for three species in one site (Ge, Cu atoms, and vacancies) is not feasible, the Cu content in the 6*d* site was fixed in consistency with EPMA data. Refinement of the Ge-content in this site consequently yields the amount of vacancies (see Table 2 and Fig. 3). It should be emphasized that compositions resulting from refinements of X-ray single crystal and powder diffraction data are in fine agreement with overall EPMA data. To elucidate the distribution of vacancies as a function of *M*-content (*M* = Pd, Pt, Cu, Cd, and Zn; see Fig. 3) we have plotted the number of vacancies per formula unit for two limit models of *M*-atom incorporation in the lattice of Ba_8Ge_{43}. Model A corresponds to *M*/Ge substitution at a constant level of vacancies (3 voids per formula as observed in binary $Ba_8Ge_{43}\square_3$ [18]) leading to a formula $Ba_8M_xGe_{43-x}\square_3$. Model B assumes that Cu-atoms first fill the three empty lattice sites and only then Cu-atoms substitute for germanium atoms. Thus model B adheres to the formula $Ba_8Cu_{3+x}Ge_{43-x}$. Whereas experimental data for *M* = Cd and Zn [6,7] clearly show a behaviour intermediate between these two models, incorporation of copper atoms is closer to model B following the line for Pt [9], i.e. at about 5.5 Cu-atoms per formula unit are needed to entirely fill vacancies at simultaneous substitution of Ge-framework atoms. At higher Cu-concentrations (up to 6 Cu-atoms/unit cell) Cu replaces Ge-atoms with all vacancies kept filled. The combined mechanisms of vacancy-filling and simultaneous Cu for Ge substitution define the lattice parameter variation as a function of Cu-content. At small

Table 2
X-ray single crystal data for $Ba_8Cu_xGe_{46-x-y}\square_y$ at $x = 2.1, 4.5, 6.0$.

Parameter/compound	$Ba_8Cu_2Ge_{44}$	$Ba_8Cu_4Ge_{42}$	$Ba_8Cu_6Ge_{40}$
Formula from refinement	$Ba_8Cu_{2.1}Ge_{41.8}\square_{2.1}$	$Ba_8Cu_{4.5}Ge_{40.9}\square_{0.6}$	$Ba_8Cu_{6.0}Ge_{40.0}$
Composition (EPMA, at.%)	$Ba_{14.9}Cu_{4.0}Ge_{81.1}$	$Ba_{14.5}Cu_{8.2}Ge_{77.3}$	$Ba_{14.5}Cu_{10.9}Ge_{74.6}$
Crystal size	$42 \times 56 \times 50\,\mu m^3$	$42 \times 56 \times 50\,\mu m^3$	$42 \times 56 \times 50\,\mu m^3$
a (nm)	1.06717(2)	1.06952(2)	1.06903(2)
a (nm), Ge standard	1.06671(3)	1.06889(2)	1.06868(2)
μ_{abs} (mm^{-1})	32.71	34.55	35.44
Data collection, 2Θ range (deg)	$2 \leqslant 2\Theta \leqslant 72.5$; 75 s/frame	$2 \leqslant 2\Theta \leqslant 72.5$; 75 s/frame	$2 \leqslant 2\Theta \leqslant 72.5$; 75 s/frame
Total number of frames	210 5 sets	210 5 sets	210 5 sets
Reflections in refinement	$455 \geqslant 4\sigma(F_o)$ of 561	$471 \geqslant 4\sigma(F_o)$ of 564	$471 \geqslant 4\sigma(F_o)$ of 564
Mosaicity	<0.43	<0.43	<0.43
Number of variables	25	25	16
$R_F^2 = \Sigma\lvert F_o^2 - F_c^2\rvert / \Sigma F_o^2$	0.0321	0.0310	0.0289
R_{Int}	0.0210	0.0183	0.0191
$wR2$	0.0350	0.0304	0.0369
GOF	1.076	1.179	1.089
Extinction (Zachariasen)	0.00057(6)	0.00084(5)	0.0011(1)
Ba1 in 2a (0,0,0); occ.	1.00(1)	1.00(1)	1.00(1)
$U_{11} = U_{22} = U_{33}$ (in $10^2 nm^2$)	0.0110(1)	0.0107(1)	0.0104(1)
Ba2 in 6c $(\frac{1}{4}, 0, \frac{1}{2})$; occ.	1.00(1)	1.00(1)	1.00(1)
U_{11}; $U_{22} = U_{33}$	0.0247(3); 0.0393(2)	0.0250(3); 0.0413(2)	0.0212(2); 0.0393(2)
M1 in 6d $(\frac{1}{4}, \frac{1}{2}, 0)$; occ.	0.357Cu[a]+0.297(3)Ge+0.346□	0.752Cu[a]+0.153(4)Ge+0.095□	1.00(1)Cu
U_{11}; $U_{22} = U_{33}$	0.0135(5); 0.0101(4)	0.0144(4); 0.0097(3)	0.0118(3); 0.0091(2)
Ge2 in 16i (x,x,x) ; occ.	1.00(1)	1.00(1)	1.00(1)
x	0.18350(2)	0.18343(2)	0.18315(2)
$U_{11} = U_{22} = U_{33}$; $U_{23} = U_{13} = U_{12}$	0.0124(1); −0.0020(1)	0.0103(1); −0.0012(1)	0.0091(1); −0.0008(1)
Ge31 in 24k (0,y,z); occ.	0.746(4)	0.885(4)	1.00(1)
y; z	0.1172(1); 0.3116(1)	0.1189(4); 0.3127(3)	0.11961(3); 0.31477(3)
U_{11}; U_{22}	0.0127(1); 0.0153(4)	0.0093(7); 0.0110(6)	0.0103(2); 0.0104(2)
U_{33}; U_{23}	0.0145(5); 0.0015(3)	0.0088(4); 0.0008(4)	0.0101(2); 0.0004(1)
Ge32 in 24k (0,y,z); occ.	0.254(4)	0.115(4)	–
y; z	0.1327(4); 0.3386(3)	0.1234(9); 0.3218(8)	–
U_{11}; U_{22}	0.0127(1); 0.0153(4)	0.016(2); 0.023(3)	–
U_{33}; U_{23}	0.0145(5); 0.0015(3)	0.033(3); 0.009(2)	–
Residual density (e^-/nm^3); max; min	1280; −1170	1050; −750	1340; −1110
Principal mean square atomic displacements U_{ij}	Ba1 0.0110 0.0110 0.0110	Ba1 0.0106 0.0106 0.0106	Ba1 0.0104 0.0104 0.0104
	Ba2 0.0393 0.0393 0.0246	Ba2 0.0411 0.0413 0.0248	Ba2 0.0393 0.0393 0.0212
	M1 0.0135 0.0101 0.0101	M1 0.0143 0.0097 0.0097	M1 0.0118 0.0091 0.0091
	Ge2 0.0144 0.0144 0.0085	Ge2 0.0114 0.0114 0.0077	Ge2 0.0099 0.0099 0.0074
	Ge31 0.0164 0.0134 0.0127	Ge31 0.0132 0.0111 0.0101	Ge3 0.0107 0.0104 0.0098
	Ge32 0.0164 0.0134 0.0127	Ge32 0.0132 0.0111 0.0101	

Room temperature, ω-scans, scan width 2°; redundancy >10; clathrate–type I; space group $Pm\bar{3}n$; no. 223; standardized with program *Structure Tidy* [26].
[a] Fixed after EPMA.

Cu-concentrations vacancy filling by Cu-atoms in the 6*d*-sites dominates and thus the lattice parameters rise with Cu-content although the Cu-atoms are smaller than Ge-atoms. Consequently, when all vacancies are filled at about 5.5 Cu-atoms per formula unit, further Ge/Cu substitution causes the lattice to shrink. The two competing influences result in a flat maximum of the lattice parameters vs. Cu-content at about $Ba_8Cu_{5.3}Ge_{40.7}$. Fig. 2 shows the lattice parameters versus Cu-content in comparison with data reported in literature. There is fine agreement of our lattice parameter data with the parameters for the small homogeneity region of binary $Ba_8Ge_{43}\square_3$ [17,18], for $Ba_8Cu_6Ge_{40}$ [11,13,15,16] as well as for the Cu-rich region $Ba_8Cu_xGe_{46-x}$ ($5.7 \leqslant x \leqslant 6.0$, [15]). It is, however, unclear how the large unit cell parameters could be obtained for binary $Ba_8Ge_{43}\square_3$ by [2] as well as for alloys $x = 2$ and 4 by [13]. Assuming strictly mono-valent Cu-atoms in the clathrate, the Zintl-scheme would be fulfilled at exactly 5.33 Cu-atoms per formula unit in perfect agreement with the experimental observation and its error bars.

With respect to the fact that for binary $Ba_8Ge_{43}\square_3$ we always observe the $a' = 2a$ supercell (which for $x \geqslant 2$ is never observed in X-ray single crystal or powder data), we conclude that the section $Ba_8Cu_xGe_{46-x}$ either exhibits a second order transformation at $0 < x < 2$ or contains a narrow two-phase field between the two structure modifications which are related by a crystallographic group–subgroup relationship.

Single crystal X-ray data refinement reveals a large anisotropy of electron densities in two cases: (i) Ba2 atoms in the 6*c* site and (ii) Ge atoms in the 24*k* site (Ge3). Consistent with earlier observations in $Ba_8M_xGe_{46-x}\square_y$ (M = Pd, Pt, Cd, and Zn [6–10]) the electron density of Ba2 atoms in the big tetrakaidecahedral cages of the Ge-framework adopts the form of a flattened rotational ellipsoid with much higher volume than that for rather isotropic Ba1 atoms in the smaller pentagondodecahedral cages of the clathrate lattice which do not show a thermal displacement factor enhanced over the general ADP values for framework atoms. Thus, in contrast to Ba2, no special rattling effect can be seen for Ba1-atoms. A plot of the electron density for the Ba2-atom at 300 K (difference Fourier synthesis $F_{obs-Ba2}$), as shown in Fig. 4, revealed a rather uniform and round shape with very little hints towards off-centre positions of the Ba2-atom. Off-centre behaviour was recently reported from X-ray powder diffraction of $Ba_8Cu_6Ge_{40}$ [16].

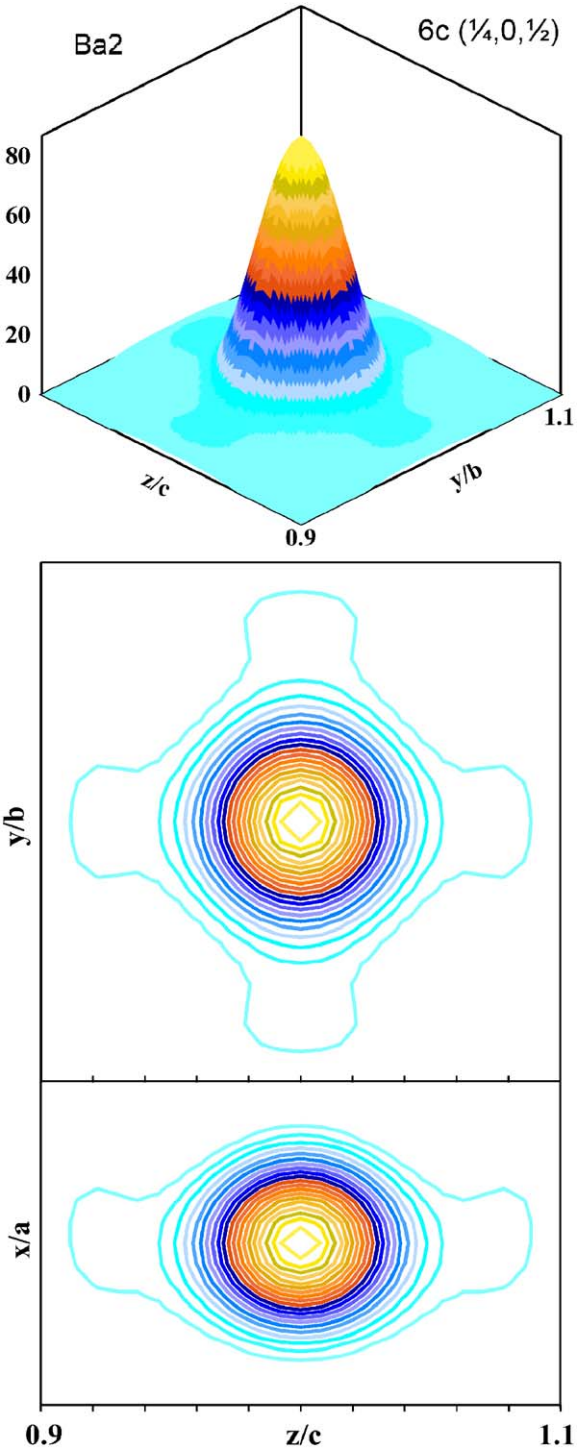

Fig. 4. Electron density at 300 K for Ba2-atom in $Ba_8Cu_6Ge_{40}$ from difference Fourier $F_{obs-Ba2}$ (top: three-dimensional view, bottom two-dimensional projections).

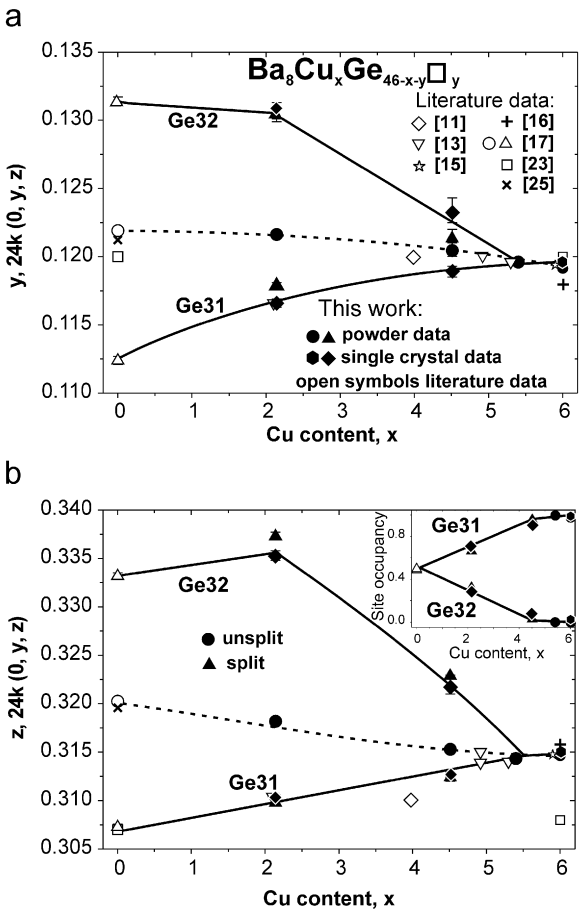

Fig. 5. Compositional dependence of positional parameters y (a) and z (b) for the Ge3-site (24k (0,y,z)) in $Ba_8Cu_xGe_{46-x-y}\square_y$. Filled symbol—our data, open symbols—literature data [24,25].

As a general feature of clathrates $Ba_8M_xGe_{46-x}\square_y$ the shape of the 24k site (Ge3) electron density adopts an ellipsoid elongated along the direction of the Ge1–Ge3 bonds proposing a split into two 24k sites (occGe31+occGe32 = 1) similar also to binary Ba_8Ge_{43} [18]. The split correlates directly with the number of vacancies in the 6d site as the electron density centred at 24k adopts a regular shape for vacancy-free compositions of $x \geqslant 5.5$ (see Fig. 5). Adopting split atom positions in the refinements reduces the reliability factors from about 4.5% to 3% and the residual electron densities reduce from 5000 to less than 1500 e^-/nm^3 finally yielding featureless difference-Fourier maps $F_{obs}-F_{calc}$. The small difference among the atomic radii of Cu and Ge are reflected in an insignificant variation of the crystallographic parameters with Cu-content (lattice parameter, atomic coordinates, and site occupancy). The results of the refinements are listed in Table 2 and Fig. 5. Interatomic distances monotonically follow the trend defined by the unit cell dimensions and atom coordinates (Fig. 6).

4. Conclusion

Phase relations involving the Ba–Cu–Ge clathrates are presented by isothermal sections at 700 and 800 °C and a solidus projection for the region $BaGe_2$–Ge–Cu_3Ge. The phase equilibria were derived by means of X-ray powder and single crystal diffractions, electron probe microanalysis and differential thermal analysis on alloys in as-cast and annealed state. Despite a limited stability range of binary clathrate type I ($Ba_8Ge_{43}\square_3$), the ternary phase $Ba_8Cu_xGe_{46-x-y}\square_y$ has an extended homogeneity region and primary crystallization field. The solid solution Ba_8Cu_x-$Ge_{46-x-y}\square_y$ extends up to $x = 6$ and adopts a cubic primitive symmetry with the space group type $Pm\bar{3}n$ consistent with a clathrate type I structure throughout the entire homogeneity region $0 < x \leqslant 6$. X-ray single crystal refinements show that incorporation of copper atoms into $Ba_8Ge_{43}\square_3$ is similar to that observed for Pt [9], but in contrast to $Ba_8Pt_xGe_{46-x-y}\square_y$ defect-free $Ba_8Cu_xGe_{46-x}$ crystallizes for $x \geqslant 5.5$. The ternary clathrate

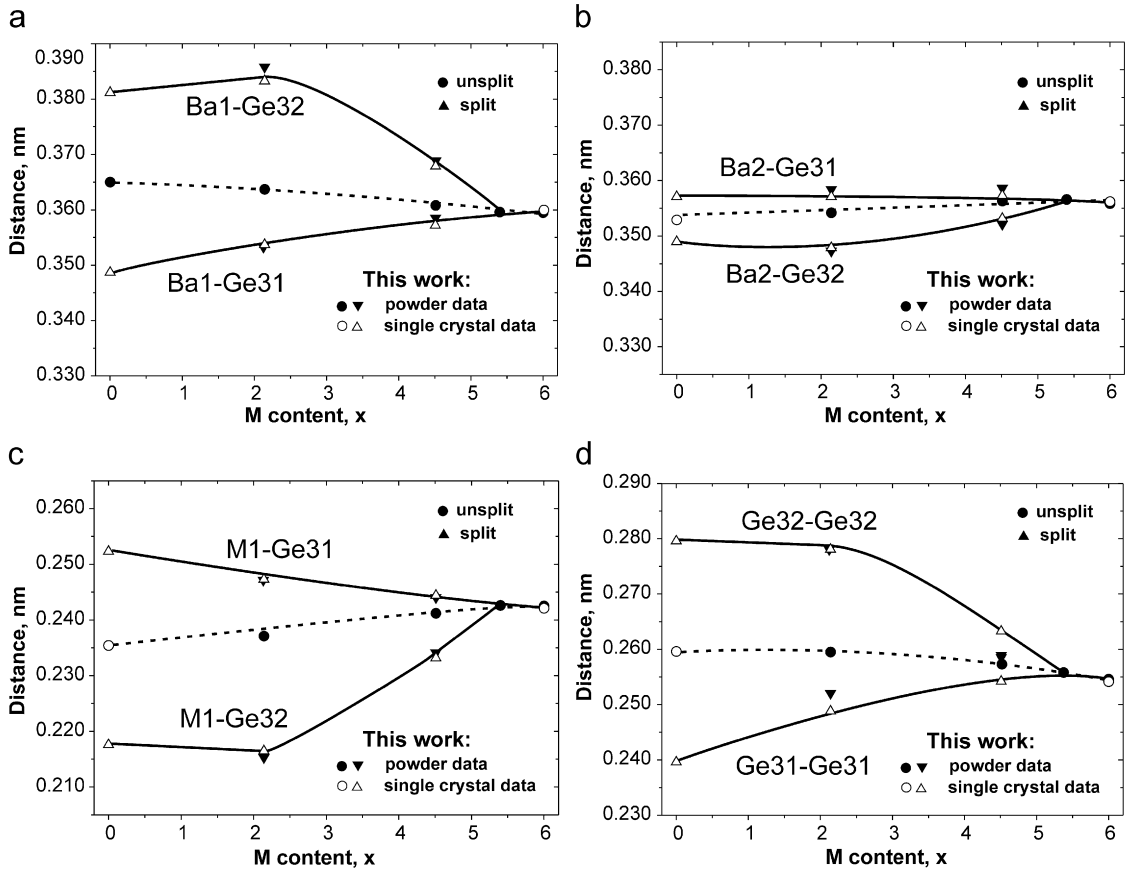

Fig. 6. Selected interatomic distances for Ba1–Ge3 (a), Ba2–Ge3 (b), Cu1–Ge3 (c), and Ge3–Ge3 (d) in $Ba_8Cu_xGe_{46-x-y}\square_y$. Filled symbols—this work, open symbols—[17] for Ba_8Ge_{43}.

phase type IX, $Ba_6(Ge_{1-x}Cu_x)_{25}$, has only a limited region $x<0.4$ in the ternary system. At 700 °C the clathrate type I solid solution is stable for $2.4\leqslant x\leqslant 6$.

Acknowledgments

The research reported herein was supported by the FFG project THECLA and the Austrian FWF projects P19165 and P16778-No2.

Appendix A. Supplementary material

Supplementary data associated with this article can be found in the online version at doi:10.1016/j.jssc.2009.04.006.

References

[1] H. Fukuoka, J. Kiyoto, S. Yamanaka, J. Phys. Chem. Solids 65 (2–3) (2004) 333–336.
[2] Y. Li, Y. Liu, N. Chen, G. Cao, Z. Feng, J.H. Ross Jr., Phys. Lett. A 345 (2005) 398–408.
[3] K. Akai, G. Zhao, K. Koga, K. Oshiro, M. Matsuura, in: Proceedings of 24th International Conference on Thermoelectrics, Beijing, China, IEEE, Piscataway, NJ, USA, 2005, pp. 230–233.
[4] K. Akai, K. Koga, M. Matsuura, Mater. Trans. 48 (4) (2007) 684–688.
[5] D.M. Rowe, Thermoelectric Handbook, Macro to Nano, CRC Press, Boca Raton, 2006 (Chapters 32 and 33).
[6] N. Melnychenko-Koblyuk, A. Grytsiv, S. Berger, H. Kaldarar, H. Michor, F. Röhrbacher, E. Royanian, E. Bauer, P. Rogl, H. Schmid, G. Giester, J. Phys. Condens. Matter 19 (2007) 046203/1–046203/23.
[7] N. Melnychenko-Koblyuk, A. Grytsiv, L. Fornasari, H. Kaldarar, H. Michor, F. Röhrbacher, M. Koza, E. Royanian, E. Bauer, P. Rogl, M. Rotter, H. Schmid, F. Marabelli, A. Devishvili, M. Doerr, G. Giester, J. Phys. Condens. Matter 19 (2007) 216223/1–216223/26.
[8] N. Melnychenko-Koblyuk, A. Grytsiv, P. Rogl, M. Rotter, R. Lackner, E. Bauer, L. Fornasari, F. Marabelli, G. Giester, Phys. Rev. B 76 (14) (2007) 144118/1–144118/11.
[9] N. Melnychenko-Koblyuk, A. Grytsiv, P. Rogl, M. Rotter, R. Lackner, E. Bauer, L. Fornasari, F. Marabelli, G. Giester, Phys. Rev. B Condens. Matter Mater. Phys. 76 (19) (2007) 195124/1–195124/47.
[10] N. Melnychenko-Koblyuk, A. Grytsiv, P. Rogl, E. Bauer, R. Lackner, E. Royanian, M. Rotter, G. Giester, J. Phys. Soc. Jpn. 77 (Suppl. A) (2008) 54–60.
[11] G. Cordier, P. Woll, J. Less Common Met. 169 (2) (1991) 291.
[12] Ya. Mudryk, P. Rogl, C. Paul, S. Berger, E. Bauer, G. Hilscher, C. Godart, H. Noél, J. Phys. Condens. Matter 14 (2002) 7991–8004.
[13] Y. Li, J. Chi, W. Guo, S. Khandekar, J.H. Ross Jr., J. Phys. Condens. Matter 15 (2003) 5535–5542.
[14] S. Johnsen, A. Bentien, G.K.H. Madsen, M. Nygren, B.B. Iversen, in: Proceedings of 24th International Conference on Thermoelectrics, Beijing, China, IEEE, Piscataway, NJ, USA, 2005, pp. 226–229.
[15] S. Johnsen, A. Bentien, G.K.H. Madsen, B.B. Iversen, M. Nygren, Chem. Mater 18 (2006) 4633.
[16] H. Zhang, J.T. Zhao, M.B. Tang, Z.Y. Man, H.H. Chen, X.X. Yang, J. Alloys Compd. 476 (2009) 1–4.
[17] W. Carrillo-Cabrera, J. Curda, K. Petters, M. Baenitz, Y. Grin, H.G. von Schnering, Z. Krisallogr. 215 (2000) 321.
[18] W. Carrillo-Cabrera, S. Budnyk, Y. Prots, Y. Grin, Z. Anorg. Allg. Chem. 630 (2004) 7226.
[19] Pauling File Binaries Edition, Version 1.0, ASM Intl, Materials Park, OH, USA, release 2002/1.
[20] W. Rieger, E. Parthé, Monatsh. Chem. 100 (1969) 439–443.
[21] C. Kranenberg, A. Mewis, Z. Anorg. Allg. Chem. 629 (6) (2003) 1023–1126.
[22] T.B. Massalski, Binary Alloy Phase Diagrams, second ed., ASM International, Materials Park, OH, 1990.
[23] W. Carrillo-Cabrera, H. Borrmann, S. Paschen, M. Baenitz, F. Steglich, Y. Grin, J. Solid State Chem. 178 (2005) 715–728.
[24] N. Okamoto, K. Tanaka, H. Inui, Acta Materiala 54 (2006) 173–178.
[25] H. Fukuoka, J. Kiyoto, S. Yamanaka, J. Solid State Chem. 175 (2003) 237–244.
[26] E. Parthé, L. Gelato, B. Chabot, M. Penzo, K. Cenzual, R. Gladyshevskii, TYPIX Standardized Data and Crystal Chemical Characterization of Inorganic Structure Types, Springer, Berlin, Heidelberg, 1994.